IOP Publishing Journal of Physics B: Atomic, Molecular and Optical Physics
J. Phys. B: At. Mol. Opt. Phys. **54** (2021) 245402 (10pp) https://doi.org/10.1088/1361-6455/ac43f5

Spontaneous polarization effects on solid high harmonic generation in ferroelectric lithium niobate crystals

Tian-Jiao Shao[1,2,*], **Fang Hu**[1,2,*] **and Hong-Bo Chen**[1,2,*]

[1] School of Information Science and Engineering, NingboTech University, Ningbo 315100, People's Republic of China
[2] Zhejiang University Ningbo Institute of Technology, Ningbo 315100, People's Republic of China

E-mail: shaotj@nit.zju.edu.cn, hufang@nit.net.cn and hbchen@zju.edu.cn

Received 6 October 2021, revised 12 December 2021
Accepted for publication 16 December 2021
Published 11 February 2022

Abstract

High-order harmonic generation (HHG) in ferroelectric lithium niobate ($LiNbO_3$) is investigated theoretically by solving the semi-conductor Bloch equations. Because of the spontaneous polarization, even-order harmonics are produced in the HHG spectra of the $LiNbO_3$ crystal driven by a monochromatic multi-cycle 3300 nm laser. Our numerical calculation shows that they are originated from the suppression of one half-optical cycle HHG process in each cycle of the driving field due to the spontaneous polarization. We also illustrate that the spontaneous polarization will increase the harmonic yield and extend the maximally attainable cutoff energy at the same time. We further report that the carrier-envelope phase dependence of HHG spectra changes from a minimum period of π rad to 2π rad when the laser polarization direction is parallel/anti-parallel to the spontaneous polarization direction in $LiNbO_3$ crystal. This is promising to be utilized as an isolated attosecond pulse gating mechanism. Moreover, the two-color relative phase dependence of HHG in $LiNbO_3$ is also investigated and shows broken inversion-symmetry.

Keywords: high-order harmonic generation, ferroelectric, spontaneous polarization, attainable cutoff energy, gating mechanism, broken inversion symmetry

(Some figures may appear in colour only in the online journal)

1. Introduction

The high-order harmonic generation (HHG) is of great significance for the generation of isolated attosecond pulses [1, 2], the development of x-ray light sources in the water window region [3, 4], and for imaging the electron wavefunction [5] and ultrafast dynamics on the atto-femtosecond time scale [6, 7]. However, the yield of synthesized attosecond pulses based on HHG in the gas medium is too small to be effectively used in the attosecond-pump attosecond-probe experiment. Recently, many experiments and theoretical studies have reported that the interaction between the femtosecond lasers and crystals could also produce HHG [8, 9]. The large atomic density of crystals and the highly orientated arrangement of atoms make the solid HHG be promising as a future bright attosecond compact EUV sources. The solid HHG shows many unique aspects that differ from its counterpart in the gas medium such as double-plateau structure [10, 11], unique dependence on the ellipticity of the driving field [12, 13], the linear dependence of the cutoff energy as a function of the driving laser field strength [11, 14], and so forth. A series of recent researches found that the solid HHG can be used for characterizing the band structure [15], spatial symmetry [16], bond information [17], and laser temporal symmetry [18], the valence potential and electron density in crystals [19]. However, some physical

* Authors to whom any correspondence should be addressed.

mechanisms [14, 20, 21] and potential applications of the solid HHG have not yet been fully clarified and still need to be shed light on [22, 23].

Recently, S. Gholam-Mirzaei et al reported the orientation dependence and polarization of the solid HHG in the ferroelectric lithium niobate (LN) and even harmonics were observed in the HHG spectra driven by a monochromatic laser field [24]. The observation of even harmonics indicates a symmetry breaking either in the HHG target or the laser field. In 2016, Luu et al investigated the HHG spectra in the ZnO crystal and attribute the symmetry breaking in HHG spectra to the interference between the crystal electrons in the valence bands [25]. Jiang et al theoretically investigated even harmonic generation in ZnO along the ΓA direction, and attributed even harmonics to the phase of the transition dipole [26]. In 2018, Luu et al observed symmetry breaking in the HHG spectra driven by two-color laser in the α–SiO_2 crystal and explained that it was due to lack of inversion-symmetry caused by the polarization response [27].

Symmetry breaking was observed recently in two-color laser-induced ablation experiments in the ferroelectric LN [28] caused by the spontaneous polarization (spontaneou s permanent dipole moment). It demonstrates that the two-color relative phase dependence curve of ablation area shows only two maxima in the phase range of [0, 2π]. While it would be four maxima for an inversion-symmetric system like inert gas when phase shifts 2π rad. Similar behavior was observed in the laser-induced orientation dependent tunnel ionization in non-centrosymmetric gas molecules, which was characterized by the molecular frame photoelectron angular distributions [29].

In our work, we have studied the symmetry breaking caused by the spontaneous polarization and its effect on the solid HHG. The spontaneous permanent dipole moment, as a new type of symmetry breaking, allows even-order harmonics to be generated by a monochromatic multi-cycle laser. The spontaneous polarization leads to the temporal Stark energy shift of the bandgap. This causes the HHG dynamics to repeat in a period changing from π rad to 2π rad. As a result, even order harmonics are generated. We also illustrate that the yield of even harmonics depends sensitively on the magnitude of the spontaneous polarization.

We further used a two-cycle laser to study the carrier-envelope (CE) phase dependence of the HHG spectra in the ferroelectric LN. The spontaneous polarization leads the CE phase dependence changes from a minimum period of π rad to 2π rad. Moreover, the two-color relative phase dependence of the HHG spectra in the ferroelectric crystal LN is also investigated and shows broken inversion symmetry.

2. Theoretical details

In this work, the solid HHG simulation is performed by solving the one-dimensional semiconductor Bloch equation (SBE) [14, 15, 28]. The details of the calculations can be found in the following. Recently, a series of theoretical advances have been achieved in SBE [30–37] for revealing the importance of considering the phase of transition dipole moment (TDM) [30, 33] and the Berry connection terms [31]. The crystal momentum dependent TDM used in SBE is evaluated from the density functional theory (DFT) calculation [38]. The dephasing time term which describes the coherence between the electron and hole is chosen $T_2 = 0.5$ o.c. (5.5 fs).

In this work, the expression of the monochromatic driving laser field can be written as,

$$\mathscr{F}(t) = \mathscr{F}_0 \exp\left[-2\ln(2)t^2/\tau_0^2\right]\cos(\omega_0 t + \varphi_{\mathrm{CE}}), \quad (1)$$

where ω_0 is the frequency of the laser field, $\mathscr{F}_0$ is the amplitude, the envelope is approximated as a Gaussian shape, τ_0 is the full width at the half maximum of the temporal profile, φ_{CE} is the CE phase.

The two-color synthesized laser field can be expressed as,

$$\begin{aligned}\mathscr{F}_{\mathrm{total}}(t) = {} & \mathscr{F}_1 \exp\left[-2\ln(2)t^2/\tau_1^2\right]\cos(\omega_1 t) \\ & + \mathscr{F}_2 \exp\left[-2\ln(2)(t+t_0)^2/\tau_2^2\right]\cos\left[\omega_2 (t+t_0)\right],\end{aligned} \quad (2)$$

where $\mathscr{F}_{\mathrm{total}}(t)$ is the total field strength of the two-color field. $\mathscr{F}_1$ and $\mathscr{F}_2$ are the amplitude of the fundamental field and control field, respectively. Both the CE phase φ_{CE} of the fundamental pulse and control field are set to be zero in our work. $\varphi_r = \omega_2 t_0$ is the relative phase and t_0 is the time-delay between the two fields.

The effective bandgap can be expressed by [39],

$$E_g(\mathscr{F}) = E_g(0) - \mu\mathscr{F}(t), \quad (3)$$

where $E_g(0)$ corresponds to the field-free bandgap energy and $\mathscr{F}$(t) is the laser field inside the crystal. Equation (3) describes the temporal evolution of the spontaneous polarization induced Stark shift. In our SBE simulation, $E_g(\mathscr{F})$ is inserted through the classical action term $S(K, t)$. μ is the electric dipole, which can be deduced from the spontaneous polarization and volume of $LiNbO_3$ unit cell v_0

$$P_s = \frac{\mu}{v_0}, \quad (4)$$

where $v_0 = 103.605$ Å^3 is the volume of the rhombohedral unit cell of LN.

A sketch of the monochromatic multi-cycle driving pulse field is shown in figure 1(a). The positive and negative polarization direction of the driving laser is plotted as solid magenta and blue lines, respectively, which indicates that the polarization of laser is parallel or anti-parallel with respect to the spontaneous polarization of ferroelectric LN. The ferroelectric LN has hexagonal conventional unit cell which contains 30 atoms and belongs to the *R*3*c* space group. The conventional and rhombohedral unit cell is presented in figures 1(b) and 2(a), respectively. Figure 2(b) shows the band structure, the highest VB and lowest conduction band (CB) along the ΓZ direction of LN rhombohedral unit cell. Figure 2(c) shows the TDM between the VB and CB.

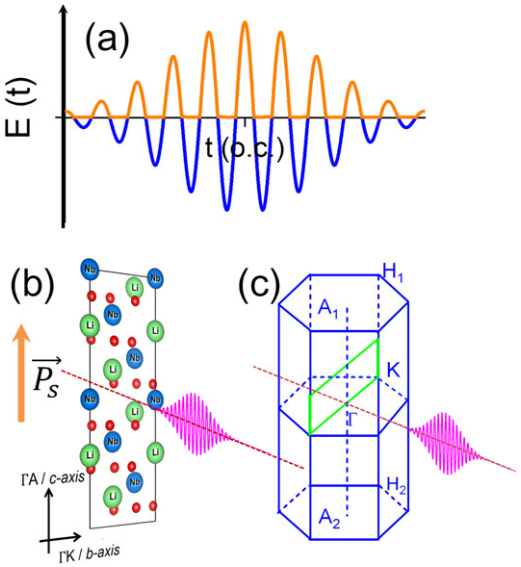

Figure 1. (a) Temporal waveform of the driving laser field. Since the laser is an alternating current field, the solid magenta line shows the field when $E(t) > 0$, the polarization direction of the laser is parallel to the spontaneous polarization P_s. While the solid blue line represents the case of $E(t) < 0$, indicating that the laser is anti-parallel to the spontaneous polarization P_s. (b) The conventional unit cell of LN. (c) The first Brillouin zone of the conventional unit cell of LN. The propagation direction of the laser is perpendicular to the Y-cut face, while the polarization direction of the laser is parallel with respect to the ΓA direction.

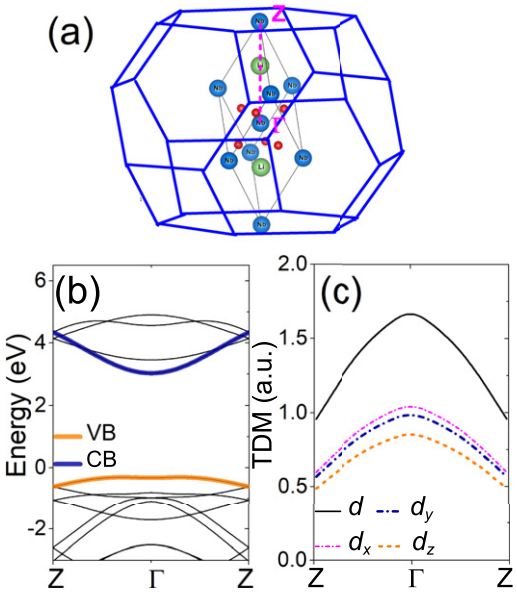

Figure 2. (a) The rhombohedral unit cell of $LiNbO_3$ and its Brillouin zone. (b) The band structure of the rhombohedral unit cell of $LiNbO_3$ along ΓZ direction. The CB minimum (CBM) and VB maximum (VBM) are plotted with solid blue line and solid orange line, respectively. (c) The total modulus of TDM (solid black line) between CBM and VBM and its component along the *kx*, *ky* and *kz* direction.

2.1. Semi-conductor Bloch equation

The electron dynamics within a solid crystal is described by the SBEs in the reciprocal momentum space, which is written in a two-band model as [49]:

$$\dot{\pi}(K,t) = -\frac{1}{T_2}\pi(K,t) - i\Omega(K,t)N(K,t)\mathrm{e}^{-\mathrm{i}S(K,t)}, \quad (5)$$

$$\dot{n}_b(K,t) = is_b\Omega^*(K,t)\pi(K,t)\mathrm{e}^{-\mathrm{i}S(K,t)} + \mathrm{c.c.}, \quad (6)$$

where $\pi(K,t)$ relates the polarization strength between the CBM and the VBM, later the polarization $p(K,t)$ is determined by $\pi(K,t)$ as

$$p(K,t) = d(K + A(t))\pi(K,t)\mathrm{e}^{\mathrm{i}S(K)} + \mathrm{c.c.}, \quad (7)$$

where T_2 and $N(K,t)$ are the polarization dephasing time and the population difference between the conduction ($n_{\mathrm{b=c}}$) and the valence ($n_{\mathrm{b=v}}$) bands, respectively. In our calculations, the dephasing time describing the coherence between these two band states is used as a free parameter and was fixed at $T_2 = 0.5$ o.c. $s_{\mathrm{b=c}} = 1$ and $s_{\mathrm{b=v}} = -1$ are constants used to describe (from unity) the band populations variation from the initial state of the system where all electrons are in the VB. $\Omega(K,t) = \mathscr{F}(t)d(K + A(t))$ is the Rabi frequency for a given laser field E(t) (with corresponding vector potential $A(t) = -\int_{-\infty}^{t}\mathscr{F}(t')\mathrm{d}t'$ and transition dipole $d(K)$. Since both the laser field $\mathscr{F}$(t) and transition dipole $d(K + A(t))$ are vectors, the $\Omega(K,t) = \mathscr{F}_x(t)d_x(K + A(t)) + \mathscr{F}_y(t)d_y(K + A(t)) + \mathscr{F}_z(t)d_z(K + A(t))$. In our case, the laser polarization is along the z-axis, therefore, $\Omega(K,t) = \mathscr{F}_z(t)d_z(K + A(t))$.

$S(K,t) = \int_{t_b}^{t}E_g(K + A(t'))\mathrm{d}t'$ is the classical action for an electron with crystal momenta K transformed into a moving frame $K = K + A(t)$, and E_g being the bandgap energy, t_b is beginning time of the laser pulse. The transition dipole can be expressed by $d(k) = i\int \mathrm{d}^3u^*_{v,k}(x) \bigtriangledown u^*_{c,k}(x)$ with $u_{m,k}$ being the periodic part of the solution of the Bloch equation.

2.2. Spontaneous polarization in $LiNbO_3$

The spontaneous polarization is tied to atomic displacement in the lattice which cause the crystal structures with broken symmetry. Then the polarization is defined as its difference between the initial state and the final states [50]. A modern definition of the polarization is as follows

$$P_{\mathrm{eff}} = P_{\mathrm{ion}} + \Delta P_{\mathrm{el}}, \quad (8)$$

where P_{ion} is the contribution from ions which can be described by classical point charge. ΔP_{el} is the electronic contribution to the spontaneous polarization and must be managed with quantum mechanics by considering the summation of all the occupied electric states [50].

The spontaneous polarization of $LiNbO_3$ is given by the equation (4). The reported magnitude of spontaneous polarization $|P_s|$ ranges from 0.6 C m^{-2} to 0.8 C m^{-2} [40–42]. In this work, except as noted, $|P_s| = 0.6$ C m^{-2} is used. The values are reported in table 1.

Figure 3 shows the temporal evolution of the spontaneous polarization induced Stark shift. In our two-band model, E_g is inserted into the SBEs through the classical action $S(K,t)$. The atomic displacement causes the change of polarization in ferro-electric crystal. The lattice displacement time is on the

Table 1. P_s in $LiNbO_3$ rhombohedral cell.

Spontaneous polarization P_s (C m^{-2})	Unit cell Volume (Å^3)	μ (C m)	μ (a.u.)
0.3	103.605	3.10815×10^{-29}	3.66598
0.6	103.605	6.21630×10^{-29}	7.33197

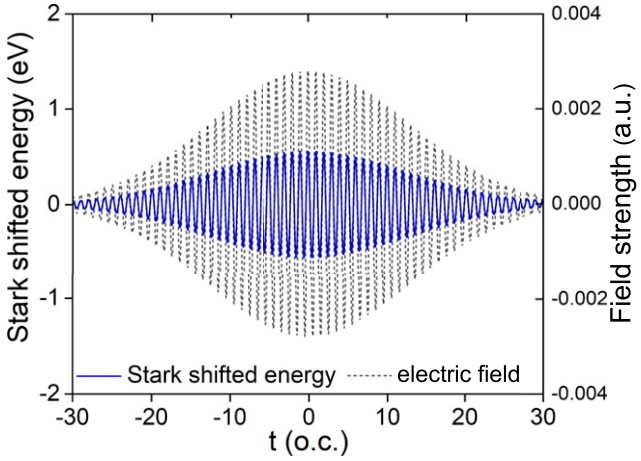

Figure 3. Predicted Stark shifted energy from equation (3). The black dashed line is the temporal profile of driving laser field. The solid blue line is the temporal evolution of the spontaneous polarization induced Stark shift. Laser parameters: $\tau_0 = 30.0$ o.c., 3300 nm pulse, field strength $E_0 = 0.0028$ a.u.

timescale of picosecond [51], as a result, we neglect the change of spontaneous polarization induced by the strong driving laser in this work.

2.3. First-principles calculations

In order to obtain the band structure and the transition dipole information of the primitive unit cells of $LiNbO_3$, the first-principles calculations were performed by using the Vienna *ab initio* simulation package (VASP) [38], the eigenvalues and eigenfunctions of the periodic system are obtained by solving the Kohn sham equations. The transition dipole moments are obtained by using the post-processing program VASP-KIT [45]. The local density approximation (LDA) is used to describe the exchange correlation function.

The full potential projection enhanced wave (PAW) method is used to describe the ion-electron interactions with a plane-wave cutoff of 500 eV. In the self consistent cycle, the Brillouin zone is sampled by a $8 \times 8 \times 8$ Monkhorst-Pack k-point mesh for the self-consistent converged calculation of charge density and wavefunction.

The LN rhombohedral cell has 10 atoms. We perform the first-principles calculations by the VASP [38], which self-consistently solve the Kohn–Sham equations for eigenvalues and eigenfunctions of the periodical system. The LDA is chosen for describing exchange–correlation functional. The projector augmented wave (PAW) formalism is used to describe the ion–electron interactions. An energy cutoff of 500 eV for plane-waves is used throughout all calculations.

Table 2. Bands expansion coefficients of the $LiNbO_3$ rhombohedral unit cell along ΓZ.

j	α_{VB}	α_{CB}	d_z (atomic units)
α_0	-0.3867	3.59	0.7051
α_1	0.112	-0.5897	0.1576
α_2	-5.812×10^{-2}	7.873×10^{-2}	-2.425×10^{-2}
α_3	1.401×10^{-2}	-3.528×10^{-2}	1.580×10^{-2}
α_4	-1.024×10^{-2}	1.977×10^{-2}	-5.378×10^{-3}
α_5	6.009×10^{-3}	-1.273×10^{-2}	4.883×10^{-3}
α_6	-4.349×10^{-3}	8.923×10^{-3}	-2.530×10^{-3}
α_7	3.254×10^{-3}	-6.727×10^{-3}	1.830×10^{-3}
α_8	-2.525×10^{-3}	5.21×10^{-3}	-1.063×10^{-3}
α_9	2.073×10^{-3}	-4.273×10^{-3}	1.094×10^{-3}
α_{10}	-1.705×10^{-3}	3.521×10^{-3}	-8.465×10^{-4}

We build the LN unit cell through experimentally measured parameters. The volume and internal ion coordinate of the unit cell are fully relaxed with respect to the pseudo-potential. A k-grid of $8 \times 8 \times 8$ was used for relaxing the unit cell to the equilibrium position. The optimized lattice ($a = 5.0979$ Å, $c = 13.8100$ Å), accords with experimental reported lattice ($a = 5.148$ Å, $c = 13.863$ Å). In the self-consistent cycle, the Brillouin zone of the unit cell is sampled by a $8 \times 8 \times 8$ k-grid for obtaining converged charge density and wavefunction. An indirect bandgap of 3.3343 eV is obtained which accords with the reported bandgap by experiment [46] and DFT [47, 48].

The band dispersion curves in the reciprocal space are originally computed from VASP and fitted by Fourier series

$$E_{CB}(t) = E_g + \sum_{j=0}^{\infty} \alpha_{CB}^{j} \cos(jk_x a_x), \tag{9}$$

$$E_{VB}(t) = +\sum_{j=0}^{\infty} \alpha_{VB}^{j} \cos(jk_x a_x), \tag{10}$$

where $a_x = 8.6985$ a.u. is the length of the lattice and k_x is the Bloch vector. We use j up to $n = 10$ along the ΓZ direction to expand the band dispersion curves. The coefficients can be found in table 2. The laser polarization is chosen to be along the ΓZ direction with $a_x = 8.6985$ Bohr for the optimized unstrained $LiNbO_3$ cell. The SBEs are solved by the finite difference method with 300 k-space points (full Brillouin zone) along ΓZ. The band structure and TDM of $LiNbO_3$ are displayed in figures 2(b) and (c).

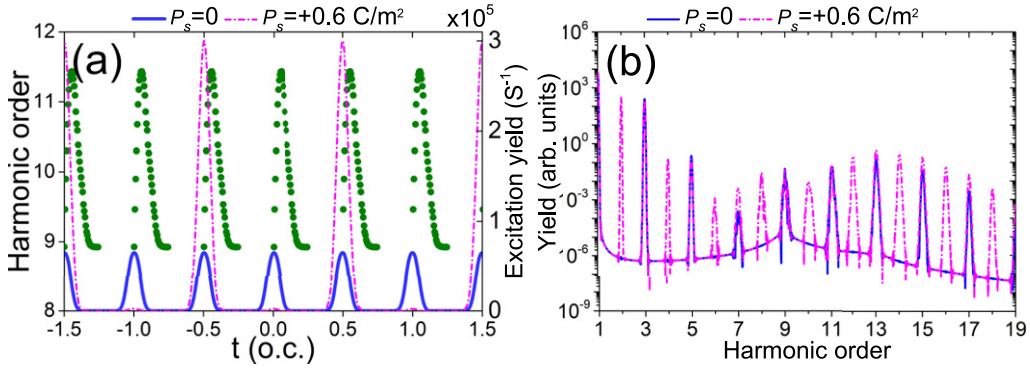

Figure 4. (a) Classical trajectories of recollision energy of solid HHG of the LN. The solid blue line and dashed-dotted magenta line show the excitation rate for $P_s = 0$ and $P_s = -0.60$ C cm^{-2}, respectively. (b) HHG spectra of the LN for $P_s = 0$ (solid blue line) and $P_s = -0.60$ C cm^{-2} (dashed-dotted magenta line). Laser parameters: $\tau_0 = 30.0$ o.c., 3300 nm pulse, field strength $E_0 = 0.0028$ a.u.

3. Results and discussion

3.1. Spontaneous polarization effects on the excitation and temporal profile of HHG

In the following, our calculation reports the spontaneous polarization effects on the excitation and the solid HHG. In our simulation, a 30 o.c., $E_0 = 0.0028$ a.u., 3300 nm monochromatic laser is employed as the driving field. Figure 4(a) shows the recollision energy of the electrons and holes, and the excitation rates varying with the tunneling time calculated by the full Keldysh model [43, 44]. The solid blue line and dashed-dotted red line shows the excitation rates of LN for $P_s = 0$ and $P_s = -0.60$ C cm^{-2}, respectively. When the direction of the electric field is anti-parallel with respect to the spontaneous polarization, the excitation rate decreases due to the increase of bandgap energy according to equation (5). For a spontaneous polarization free system, the solid blue line shows the excitation occurs at the peak of field. By assuming a spontaneous polarization $P_s = -0.6$ C m^{-2}, in each optical cycle of the laser field, one excitation peak is suppressed due to the opposite direction between the laser and the spontaneous polarization, while excitation in its neighboring half optical cycle is enhanced. This explains why sharp even harmonics emerge in the HHG spectra for $P_s = -0.6$ C m^{-2} (dashed-dotted magenta line) in figure 4(b). While all even harmonics almost disappear in the HHG spectra for $P_s = 0$ (solid blue line).

Figures 5(a), (c) and (e) show the interband and intraband contributions of HHG in the LN by assuming $P_s = 0$ (a), $P_s = -0.06$ C m^{-2} (c) and $P_s = -0.6$ C m^{-2} (e), respectively. Firstly, the HHG yield contributed by the interband transition is much larger than the intraband transition for the harmonic energy above the minimum bandgap (dashed-dotted green line). Second, even harmonics are observed in both interband and intraband HHG spectra for $P_s = -0.06$ C m^{-2} (c) and $P_s = -0.6$ C m^{-2} (e).

Figures 5(b), (d), and (f) show the temporal harmonic profile of interband transition for $P_s = 0$, $P_s = -0.06$ C m^{-2} and $P_s = -0.6$ C m^{-2}, respectively. The HHG photon energy (grey and green scatters) was plotted as a function of recombination time by using the saddle-point semiclassical equation for the motion of electron/hole. In figure 5(d), when the spontaneous polarization $P_s = -0.06$ C m^{-2} is assumed, in each optical cycle, one harmonic burst is suppressed due to the decrease of excitation rates of the electron-hole pairs. In figure 5(f), when the spontaneous polarization increases to $P_s = -0.6$ C m^{-2}, the harmonic burst in 'suppressed' cycle is further reduced. This breaks the intrinsic temporal symmetry of the HHG process, changes the minimum period of HHG emission from half optical cycle figure 5(b) to one optical cycle figures 5(d) and (f). This explains why the even harmonics emerge in the frequency domain.

3.2. Spontaneous polarization effects on the cutoff energy of HHG

In addition, the spontaneous polarization will have small influence on the maximally attainable cutoff energy. Both cutoff energy and yield increases (decreases) in the 'enhanced' ('suppressed') half-cycle due to spontaneous polarization effects. Figure 6(a) shows the recollision energy varies with tunneling (green solid rounds) and recombination time (red balls) by considering Stark-energy shift at the electron–hole recombination stage.

Generally speaking, the electrons contribute to the cutoff energy are ionized near the peak of the driving light field. The cutoff electrons usually return and re-collide with the holes when the electric field is close to zero (3/4 optical cycle after its ionization). Thus the Stark effect affects the excitation rate of the electrons and the harmonic yield a lot. Since the electric field is close to zero at the recombination time, the Stark energy shift is small. Therefore, compared with the excitation process, the cutoff energy of HHG is less influenced.

We found the energy of attainable cutoff harmonic photon will be slightly improved as shown in figure 6(a). For the 'enhanced' half-cycle, the excitation rate of electrons contribute to the harmonic cutoff is improved. When the electrons recombine, the polarization direction of the laser is reversed, the Stark-shifted energy is positive as shown in figure 6(b). Therefore, the cutoff energy is slightly improved. However, for the 'suppressed' half-cycle, the excitation rates of electrons decrease due to positive Stark-shifted energy

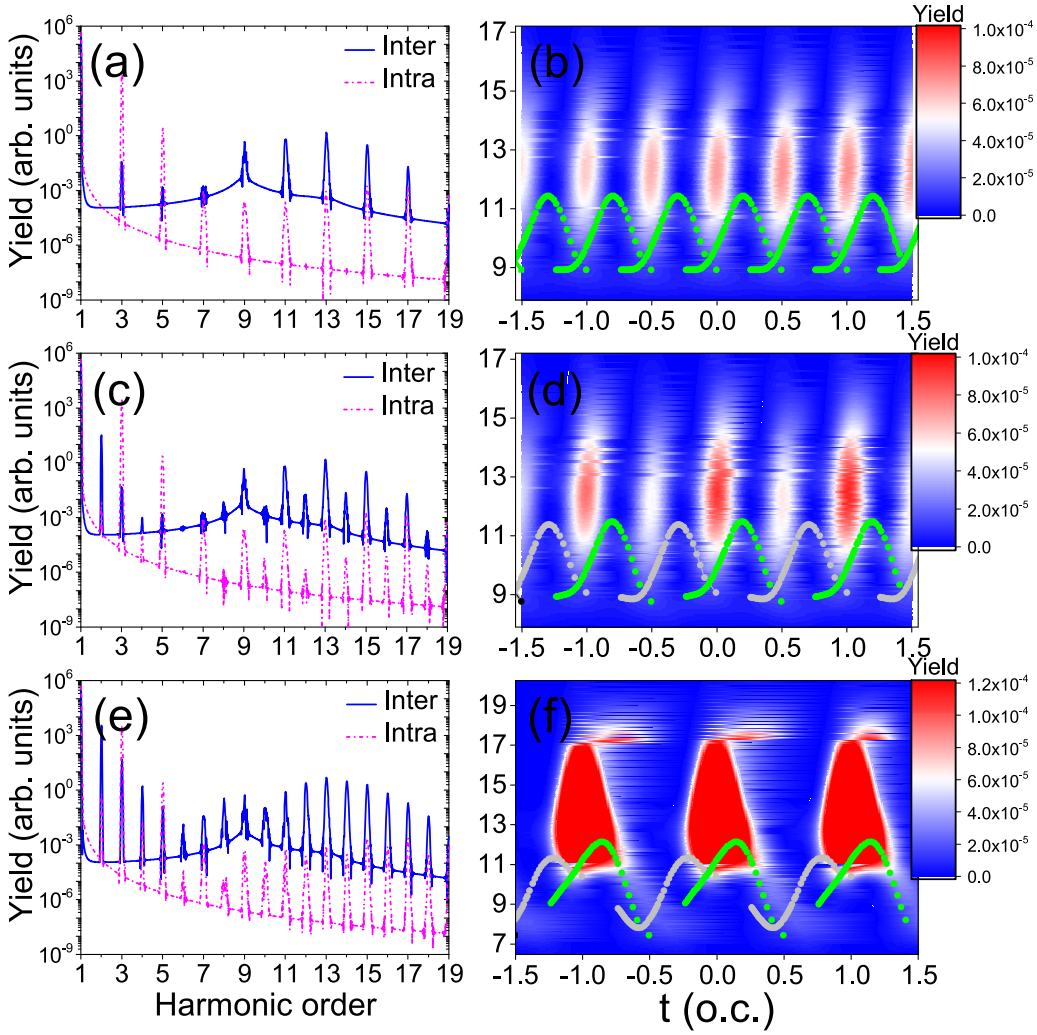

Figure 5. (a), (c) and (e) Expected interband and intraband contributions for $P_s = 0$ (a), -0.06 C m^{-2} (c) and -0.6 C m^{-2} (e). (b), (d) and (f) The temporal HHG profile of interband transition on the logarithm scale, for $P_s = 0$ (b), -0.06 C m^{-2} (d) and -0.6 C m^{-2} (f). The green scatters show the classical trajectories of the interband transition. The trajectory contours corresponding to the suppressed sub-cycle burst in (b) and (d) are plotted in grey scatters. Laser parameters: $\tau_0 = 30.0$ o.c., 3300 nm pulse, field strength $E_0 = 0.002\,8$ a.u. (a), (c) $P_s = 0$; (b), (d) $P_s = -0.06$ C m^2; (e), (f) P$_s = -0.6$ C m^{-2}.

of ionization time. When the electrons recombine, the polarization direction of the laser is reversed; the Stark-shifted energy is negative. Therefore, the cutoff energy of electrons in the 'suppressed' half-cycle will reduce. This is good for the synthesizing of the solid HHG source with enhanced photon energy and higher brightness at the same time.

3.3. Spontaneous polarization strength dependence

Figure 7(a) shows the spontaneous polarization strength dependence of HHG in the LN. $|P_s|$ ranges from 0 to 0.9 C m^{-2}. By increasing the spontaneous polarization strength $|P_s|$, the even harmonics are enhanced gradually. Figure 7(b) shows the yield of even harmonics increases by nearly one order when the spontaneous polarization $|P_s|$ increases from 0.3 to 0.8 C m^{-2}. Our calculation indicates that the even harmonic is sensitively dependent on the spontaneous polarization strength.

3.4. CE phase dependence

In the following, we investigate the CE phase dependence by employing a two-cycle, 3300 nm, $E_0 = 0.0028$ a.u. laser pulse.

Figure 8(a) shows the temporal waveform of a two-cycle laser pulse with $\Phi_{CE} = 0$ and $\Phi_{CE} = \pi$ rad, respectively. The two waveforms are identical except for their opposite laser polarization direction. For an inversion-symmetric system such as inert gas or fused-silica, it is expected that the two waveforms with a CE phase difference of π rad will generate the same HHG spectra. In figure 8(c), by assuming $P_s = 0$, the HHG spectra dependence on the CE phase shows a π phase periodicity which accords with our discussion above.

However, by assuming a spontaneous polarization $P_s = -0.6$ C m^{-2}, the HHG spectra for $\Phi_{CE} = 0$ and $\Phi_{CE} = \pi$ rad are clearly different as shown in figures 8(b) and (d). We can see that the CE phase dependence in figure 8(d) shows a modulation of 2π rad.

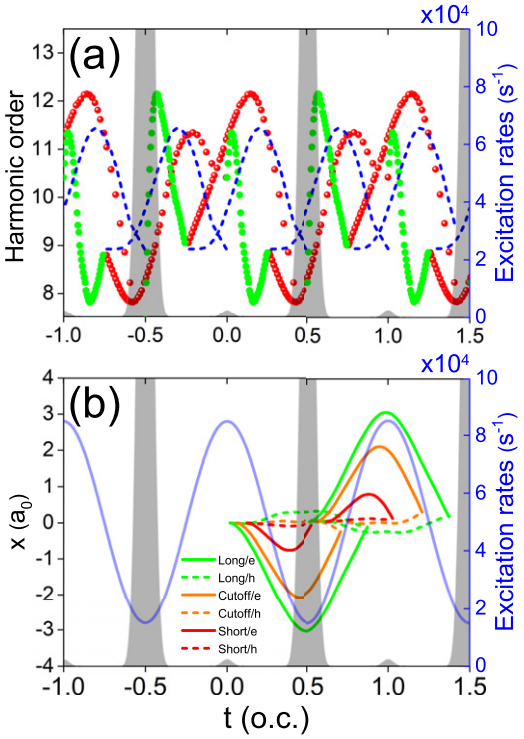

Figure 6. (a) The recollision energy varies with tunneling (green solid rounds) and recombination time (red balls) by considering the Stark-energy shift when electron and hole recombines. The case of zero spontaneous polarization is plotted with dashed blue line (only their dependence on recombination time is plotted). The excitation probability (gray filled curve) is plotted as function of time. (b) The displacement of the short trajectories of the electrons (red solid line) and holes (red dash-dotted line), long trajectories of the electrons (green solid line) and holes (green dashed line) for the 10th harmonic in real space, and the cutoff trajectory of the electrons (orange solid line) and holes (orange dashed line). The temporal profile of driving field is plotted as function of time for light blue solid line. x is the displacement of the electrons/holes in the coordinate space and a_0 is the lattice parameter. Laser parameters: $\tau_0 = 30.0$ o.c., 3300 nm pulse, field strength $E_0 = 0.002\,8$ a.u.

Figures 8(e) and (f) show the temporal harmonic profile driven by two-cycle lasers with CE phase of $\Phi_{CE} = 0$ and $\Phi_{CE} = \pi$ rad, respectively. The solid green line is the classical trajectory obtained by the saddle-point semiclassical equation of the motion of electron/hole. We can see the short and long trajectories of solid HHG in each half optical cycle in figures 8(e) and (f). The half-optical cycle harmonic emission bursts '1', '2' and '3' are marked. For $\Phi_{CE} = 0$, the harmonic burst '1' and '3' are strengthened, while harmonic emission bursts '2' is suppressed figure 8(e). On the contrary, for $\Phi_{CE} = \pi$ rad, the harmonic bursts '2' is enhanced, while harmonic burst '1' and '3' are suppressed figure 8(f). This indicates that the spontaneous polarization can be utilized to select the attosecond harmonic bursts in HHG driven by a few-cycle pulse, which might be useful for obtaining shorter and more intense isolated attosecond pulses.

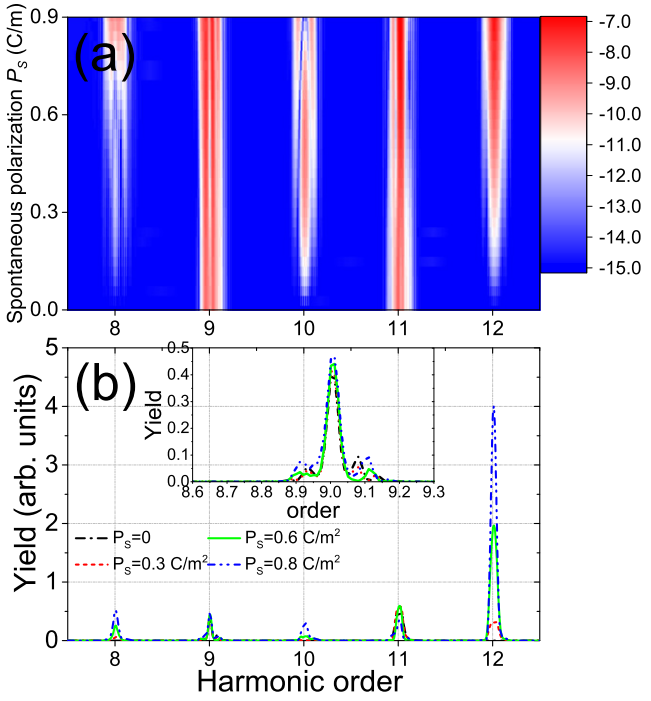

Figure 7. The spontaneous polarization strength dependence of the solid HHG spectra. (a) Predicted HHG yield as a function of the P_s. (b) The HHG spectra for $|P_s| = 0$ (dashed-dotted black line), 0.3 C m^{-2} (dashed red line), 0.6 C m^{-2} (solid green line), and 0.8 C m^{-2} (dashed-dotted blue line). Laser parameters: $\tau_0 = 30.0$ o.c., 3300 nm pulse, field strength $E_0 = 0.0028$ a.u.

3.5. *Two-color phase dependence*

In the following, our calculation presents the two-color relative phase dependence of the HHG spectra. In our simulation, the amplitudes of the fundamental pulse and the second-harmonic control pulse are $E_1 = 0.006$ a.u. and $E_2 = 0.003$ a.u., respectively. By using a phase-controlled ω–2ω two-color laser field, the temporal symmetry of half optical cycle of HHG process is destroyed. Besides the appearance of even-order harmonics, there are four oscillations per fundamental laser cycle, which is the case of HHG spectra in atomic gases. When the two-color scheme combined with medium which has spontaneous polarization, the fundamental laser field interacts spontaneous polarization and produces an asymmetry of ionization in temporal field. This asymmetry combining with the 2ω control field will generate only one maximum of HHG process per half optical cycle. Therefore, two oscillations are expected in phase-controlled HHG spectra per fundamental optical period.

Figure 9(a) shows the fundamental pulse field and second-order harmonic control field (solid orange line), with four different relative phase of $\Phi_r = 0, 0.5\pi$ rad, π rad, and 1.5π rad. When the relative phase between the fundamental field and the control field become $\Phi_r = 0$ or $\Phi_r = \pi$ rad, the upward maximum of the fundamental field will overlap with the upward maximum of the control field, which causes the total field

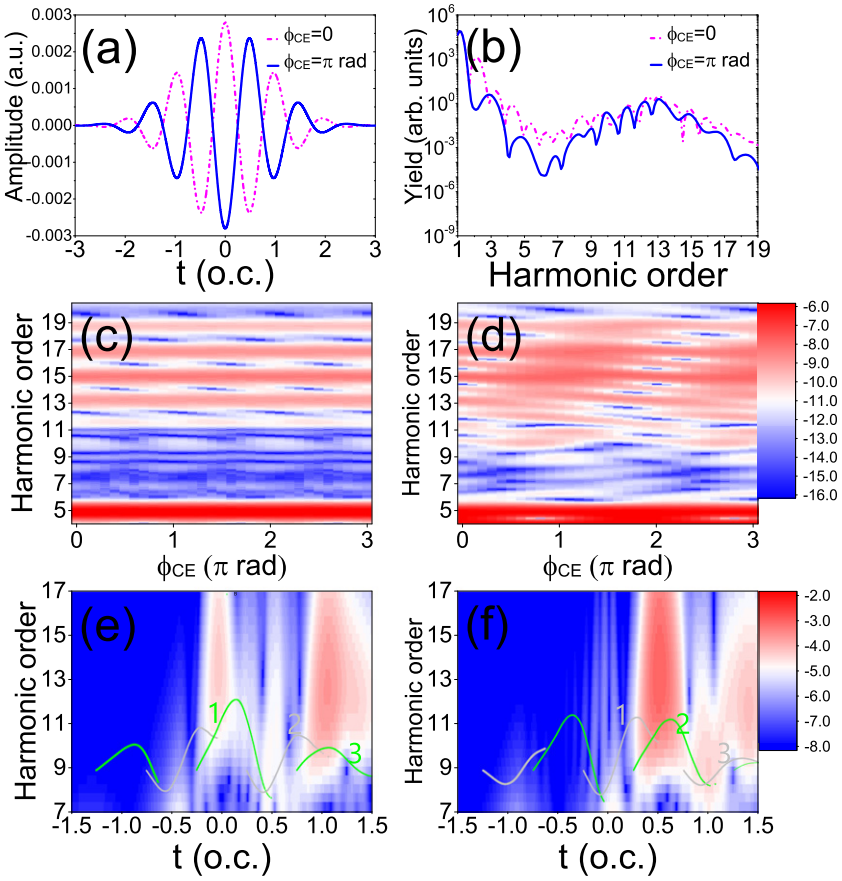

Figure 8. (a) Two-cycle pulse temporal waveform shape for two different CEP values of $\Phi_{CE} = 0$ and $\Phi_{CE} = \pi$ rad. (b) The HHG spectra for $\Phi_{CE} = 0$ (dashed-dotted magenta line) and $\Phi_{CE} = \pi$ rad (solid blue line) for LN with $P_s = -0.6$ C m^{-2}. (c) and (d) Calculated CE phase dependence of the HHG spectra by assuming $P_s = 0$ (c) and $P_s = -0.6$ C m^{-2} (d), respectively. (e) and (f) The temporal HHG profile for $\Phi_{CE} = 0$ and $\Phi_{CE} = \pi$ rad, assuming $P_s = -0.6$ C m^{-2}. Laser parameters: $\tau_0 = 2.0$ o.c., 3300 nm pulse, field strength $E_0 = 0.0028$ a.u. (c) Spontaneous polarization $P_s = 0$; (d)–(f) Spontaneous polarization $P_s = -0.6$ C m^{-2}.

reaching its upward maximum as shown by the dotted red line and dashed-dotted magenta line in figure 9(b). On the contrary, when the relative phase between the fundamental field and the control field is $\Phi_r = 0.5\pi$ or $\Phi_r = 1.5\pi$ rad, the downward maximum of the fundamental field will overlap with the downward maximum of the control field, which causes the total field reaching its downward maximum as shown by the solid blue line in figure 9(b). Therefore, for an inversion-symmetric system, when the relative phase Φ_r shifts from 0 to 2π rad, the total laser field will reach four maxima, thus the yield HHG spectra will achieve four maxima as shown in figure 9(c).

When the spontaneous polarization is assumed to be $P_s = -0.6$ C m^{-2}, the inversion symmetry is broken. When the total laser field reaches the downward maximum ($\Phi_r = 0.5\pi$ or $\Phi_r = 1.5\pi$ rad), the spontaneous polarization causes the decrease of bandgap, leading to the maximum of the yield as shown in figure 9(d). When the total laser field reaches the upward maximum ($\Phi_r = 0$ or $\Phi_r = 1.0\pi$ rad), the spontaneous polarization causes the increase of bandgap, leading to a suppression of the HHG yield. Our results accord with Luu's discussion and analysis for the phase-controlled two-color laser field driven HHG spectra in the ZnO crystal [25]. In ω–2ω two-color scheme, the broken symmetry of spontaneous polarization and the driving field competes. When the broken symmetry of spontaneous polarization is dominant, there are two oscillations per fundamental cycle as shown in figure 9(d), which are discussed above. To the opposite, when broken symmetry of temporal driving field plays a leading role and spontaneous polarization is much smaller, four oscillations are expected per fundamental laser cycle in figure 9(c).

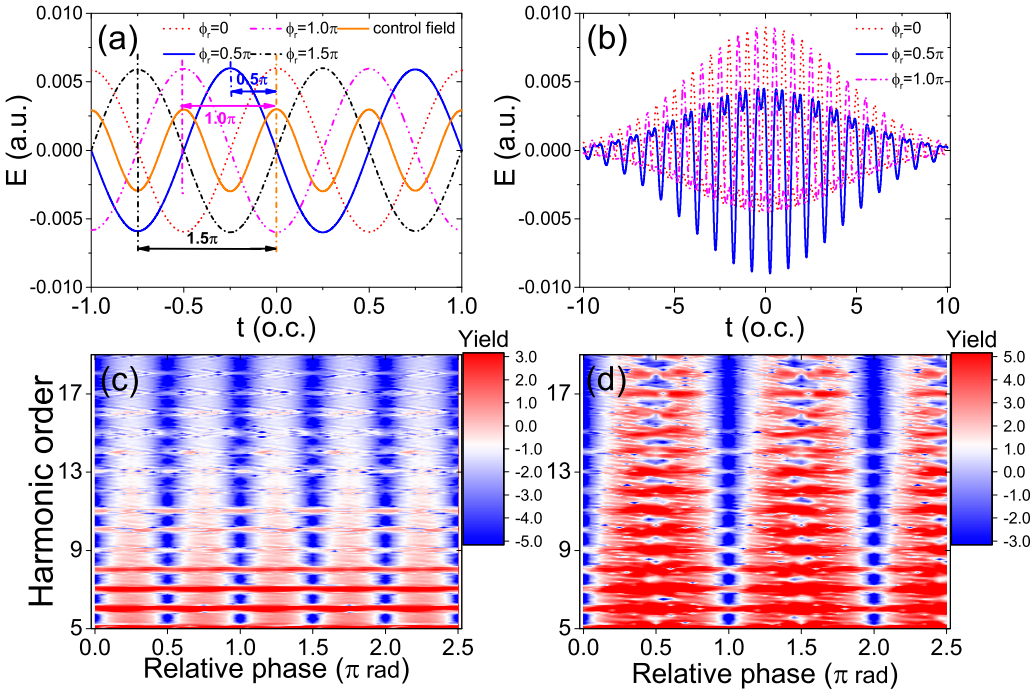

Figure 9. (a) Temporal waveform shape for the fundamental laser field and second-order harmonic control field with relative phase $\Phi_r = 0$, 0.5π rad, π rad and 1.5π rad. (b) Temporal waveform of total electric field of the two-color laser for $\Phi_r = 0$, $\Phi_r = 0.5\pi$ rad, and $\Phi_r = \pi$ rad, respectively. (c) and (d) Simulated HHG spectra of LN as a function of the two-color relative phase, assuming (c) $P_s = 0$ and (d) $P_s = -0.6$ C m^{-2}. Fundamental pulse: $\tau_1 = 10.0$ o.c., 3300 nm, $E_1 = 0.006$ a.u.; control pulse: $\tau_2 = 20.0$ o.c., 1650 nm, $E_2 = 0.003$ a.u.

4. Conclusion

The motivation of this paper is to investigate how the spontaneous polarization affects the solid HHG process. First, driven by a monochromatic multi-cycle 3300 nm laser pulse, the solid HHG spectra exhibit even order harmonics. When the spontaneous polarization is opposite to the laser polarization direction, an increase of the bandgap due to the Stark shift leads to the suppression of one half-cycle HHG process in each optical cycle and enhancement of its neighboring half-cycle HHG process. Our theoretical simulation based on the SBE confirms the selection rules of the process, and a microscopic mechanism on the basis of sub-cycle temporal gating of harmonic emission is proposed. In addition to the even harmonic generation in the ferroelectric LN, the interference should be a phenomenon occurring in other ferroelectric crystals that have permanent dipoles.

Further, we find that the spontaneous polarization will increase the harmonic yield and extend the maximally attainable cutoff energy at the same time. Our calculations show that the yield of the even harmonics increase sensitively with the enhancement of spontaneous polarization strength of solid.

We further extend the analysis to the case of few-cycle driving field controlled by CE phase and two-color field. The symmetry-breaking imposed by the laser field competes with the loss of inversion symmetry inherent to the ferroelectric system. The CE phase dependence of HHG spectra shows a minimum period of 2π rad compared to π rad in the case of HHG for an inversion-symmetric target. Through utilizing the spontaneous polarization combined with the CE phase, the quantum path of the HHG process can be effectively controlled and its possible application for the temporal gating in attosecond pulse synthesizing is discussed.

Moreover, the two-color relative phase dependence of HHG spectra shows two maxima when the phase Φ_r shifts 2π rad, in contrast, four maxima are observed in the case of an inversion-symmetric HHG target. Moreover, these effects can be developed as a promising all-optical method to characterize the CE phase of few-cycle pulse or relative phase of a two-color field.

Acknowledgments

I thank Professor Xue-Bin Bian for the discussions. This work was supported by the Ningbo Natural Science Foundation 2015A610042 and the National Natural Science Foundation of China (Grant No. 12104395).

Data availability statement

The data that support the findings of this study are available from the corresponding author upon reasonable request.

ORCID iDs

Tian-Jiao Shao https://orcid.org/0000-0001-5178-4544

References

[1] Hentschel M *et al* 2001 *Nature* **414** 509–13
[2] Paul P M, Toma E S, Breger P, Mullot G, Augeí F, Balcou P, Muller H G and Agostini P 2001 *Science* **292** 1689–92
[3] Ishii N, Kaneshima K, Kitano K, Kanai T, Watanabe S and Itatani J 2014 *Nat. Commun.* **5** 1–6
[4] Popmintchev T *et al* 2012 *science* **336** 1287–91
[5] Itatani J, Levesque J, Zeidler D, Niikura H, Pépin H, Kieffer J C, Corkum P B and Villeneuve D M 2004 *Nature* **432** 867–71
[6] Niikura H, Légaré F, Hasbani R, Bandrauk A D, Ivanov M Y, Villeneuve D M and Corkum P B 2002 *Nature* **417** 917–22
[7] Bian X-B and Bandrauk A D 2014 *Phys. Rev. Lett.* **113** 193901
[8] Burnett N H, Baldis H A, Richardson M C and Enright G D 1977 *Appl. Phys. Lett.* **31** 172–4
[9] Ghimire S, DiChiara A D, Sistrunk E, Agostini P, DiMauro L F and Reis D A 2011 *Nat. Phys.* **7** 138–41
[10] You Y S *et al* 2017 *Opt. Lett.* **42** 1816–9
[11] Ndabashimiye G, Ghimire S, Wu M, Browne D A, Schafer K J, Gaarde M B and Reis D A 2016 *Nature* **534** 520–3
[12] Yoshikawa N, Tamaya T and Tanaka K 2017 *Science* **356** 736–8
[13] Tancogne-Dejean N, Mücke O D, Kärtner F X and Rubio A 2017 *Nat. Commun.* **8** 1–10
[14] Vampa G, McDonald C R, Orlando G, Klug D D, Corkum P B and Brabec T 2014 *Phys. Rev. Lett.* **113** 073901
[15] Vampa G, Hammond T J, Thiré N, Schmidt B E, Légaré F, McDonald C R, Brabec T, Klug D D and Corkum P B 2015 *Phys. Rev. Lett.* **115** 193603
[16] Saito N, Xia P, Lu F, Kanai T, Itatani J and Ishii N 2017 *Optica* **4** 1333–6
[17] You Y S, Reis D A and Ghimire S 2017 *Nat. Phys.* **13** 345–9
[18] Neufeld O, Podolsky D and Cohen O 2019 *Nat. Commun.* **10** 405
[19] Lakhotia H, Kim H Y, Zhan M, Hu S, Meng S and Goulielmakis E 2020 *Nature* **583** 55–9
[20] Wu M, Ghimire S, Reis D A, Schafer K J and Gaarde M B 2015 *Phys. Rev.* A **91** 043839
[21] Guan Z, Zhou X X and Bian X B 2016 *Phys. Rev.* A **93** 033852
[22] Ghimire S and Reis D A 2019 *Nat. Phys.* **15** 10–6
[23] Li J, Lu J, Chew A, Han S, Li J, Wu Y, Wang H, Ghimire S and Chang Z 2020 *Nat. Commun.* **11** 1–13
[24] Gholam-Mirzaei S, Crites E, Journigan T, Turkowski V, Sjaardema T, Fathpour S and Chini M 2020 High harmonic generation from thin-film Linbo3 *Conf. on Lasers and Electro-Optics (Optical Society of America)* p JW2F.7 (http://osapublishing.org/abstract.cfm?URI=CLEO_QELS-2020-JW2F.7)
[25] Luu T T and Wörner H J 2016 *Phys. Rev.* B **94** 115164
[26] Jiang S, Chen J, Wei H, Yu C, Lu R and Lin C D 2018 *Phys. Rev. Lett.* **120** 253201
[27] Luu T T and Wörner H J 2018 *Phys. Rev.* A **98** 041802
[28] Wanie V *et al* 2020 *Phys. Rev.* B **101** 184103
[29] Akagi H, Otobe T, Staudte A, Shiner A, Turner F, Dörner R, Villeneuve D M and Corkum P B 2009 *Science* **325** 1364–7
[30] Jiang S, Wei H, Chen J, Yu C, Lu R and Lin C D 2017 *Phys. Rev.* A **96** 053850
[31] Li J, Zhang X, Fu S, Feng Y, Hu B and Du H 2019 *Phys. Rev.* A **100** 043404
[32] Silva R E F, Martín F and Ivanov M 2019 *Phys. Rev.* B **100** 195201
[33] Du M, Liu C, Zheng Y, Zeng Z and Li R 2019 *Phys. Rev.* A **100** 043840
[34] Yue L and Gaarde M B 2020 *Phys. Rev. Lett.* **124** 153204
[35] Yue L and Gaarde M B 2020 *Phys. Rev.* A **101** 053411
[36] Moos D, Jürß C and Bauer D 2020 *Phys. Rev.* A **102** 053112
[37] Wilhelm J, Grössing P, Seith A, Crewse J, Nitsch M, Weigl L, Schmid C and Evers F 2021 *Phys. Rev.* B **103** 125419
[38] Kresse G and Hafner J 1993 *Phys. Rev.* B **47** 558–61
[39] Etches A and Madsen L B 2010 *J. Phys. B: At. Mol. Opt. Phys.* **43** 155602
[40] Phillpot S R and Gopalan V 2004 *Appl. Phys. Lett.* **84** 1916–8
[41] Gopalan V, Mitchell T E, Furukawa Y and Kitamura K 1998 *Appl. Phys. Lett.* **72** 1981–3
[42] Lee D, Xu H, Dierolf V, Gopalan V and Phillpot S R 2010 *Phys. Rev.* B **82** 014104
[43] Keldysh L 1965 *Sov. Phys. JETP* **20** 1307–14
[44] Golin S M, Kirkwood S E, Klug D D, Villeneuve D M, Rayner D M, Herrero C A T and Corkum P B 2014 *J. Phys. B: At. Mol. Opt. Phys.* **47** 204025
[45] Wang V, Xu N, Liu J C, Tang G and Geng W T 2019 arXiv:1908.08269
[46] Dhar A and Mansingh A 1990 *J. Appl. Phys.* **68** 5804–9
[47] Mamoun S, Merad A E and Guilbert L 2013 *Comput. Mater. Sci.* **79** 125–31
[48] Riefer A, Friedrich M, Sanna S, Gerstmann U, Schindlmayr A and Schmidt W G 2016 *Phys. Rev.* B **93** 075205
[49] Vampa G, McDonald C R, Orlando G, Corkum P B and Brabec T 2015 *Phys. Rev.* B **91** 064302
[50] Resta R and Vanderbilt D 2007 *Phys. Ferroelectrics* 31–68
[51] Cushing S K, Zürch M, Kraus P M, Carneiro L M, Lee A, Chang H-T, Kaplan C J and Leone S R 2018 *Struct. Dyn.* **5** 054302

Web of Science™ Core Collection

经检索《Web of Science™ Core Collection》，下述论文被《SCI - Expanded》收录。（数据获取：2022年02月23日）

标题:Spontaneous polarization effects on solid high harmonic generation in ferroelectric lithium niobate crystals

作者:Shao, TJ(Shao, Tianjiao) Hu, F(Hu, Fang) Chen, HB(Chen, Hongbo)

来源出版物:JOURNAL OF PHYSICS B-ATOMIC MOLECULAR AND OPTICAL PHYSICS **卷**:54 **期**:24 **文献号**:245402

出版时间:2021,DEC 22 **DOI**:10.1088/1361-6455/ac43f5

出版商:IOP Publishing Ltd **出版商地址**:TEMPLE CIRCUS, TEMPLE WAY, BRISTOL BS1 6BE, ENGLAND

文献类型:Article **语种**:English

入藏号:WOS:000754056800001 **IDS号**:YX4DT

地址:[Shao, Tian-Jiao; Hu, Fang; Chen, Hong-Bo] NingboTech Univ, Sch Informat Sci & Engn, Ningbo 315100, Peoples R China; [Shao, Tian-Jiao; Hu, Fang; Chen, Hong-Bo] Zhejiang Univ, Ningbo Inst Technol, Ningbo 315100, Peoples R China

通讯作者:Shao, TJ; Hu, F; Chen, HB (corresponding author), NingboTech Univ, Sch Informat Sci & Engn, Ningbo 315100, Peoples R China.; Shao, TJ; Hu, F; Chen, HB (corresponding author), Zhejiang Univ, Ningbo Inst Technol, Ningbo 315100, Peoples R China.

电子邮件:shaotj@nit.zju.edu.cn; hufang@nit.net.cn; hbchen@zju.edu.cn

ISSN:0953-4075 **电子ISSN**:1361-6455

ISO 来源文献缩写:J. Phys. B-At. Mol. Opt. Phys. **来源出版物页码计数**:10

注：

以上检索结果均得到被检索人的确认。本证明编号：NBT-SCIE-2021-3356

《SCI - Expanded》检索结果（收录情况）

浙大宁波理工学院图书馆

检索人(签名)：

审核人(签章)：

2022年10月08日

InCites™ Journal Citation Reports®

经检索《Web of Science™》的JCR数据库，期刊《JOURNAL OF PHYSICS B-ATOMIC MOLECULAR AND OPTICAL PHYSICS》2021年JCR的影响因子情况：

ISSN：0953-4075

eISSN：1361-6455

2021年影响因子：1.655

PHYSICS, ATOMIC, MOLECULAR & CHEMICAL：Q3

OPTICS：Q4

注：

1.以上检索结果均得到被检索人的确认。证明编号：NBT-SCIE-2021-3356-IF2021

2.论文的期刊影响因子应与该论文所发表期刊的年份相对应。

《JOURNAL CITATION REPORTS（JCR）》检索结果

浙大宁波理工学院图书馆

检索人(签名)：

审核人(签章)：

2022年10月08日